Medical Engineering and Physics 102 (2022) 103782

Contents lists available at ScienceDirect

Medical Engineering and Physics

journal homepage: www.elsevier.com/locate/medengphy

In-vitro viability of laser cladded Fe-based metallic glass as a promising bioactive material for improved osseointegration of orthopedic implants

Mahmoud Z. Ibrahim [a,b,*], Ahmed Halilu [c], Ahmed A.D. Sarhan [d,e,**], T.Y. Kuo [f], Farazila Yusuf [b], M.O. Shaikh [g], M. Hamdi [b,***]

[a] Department of Mechanical Engineering, Faculty of Engineering, Ain Shams University, Cairo, 11517, Egypt
[b] Advanced Manufacturing & Material Processing (AMMP) Research Centre, Department of Mechanical Engineering, Faculty of Engineering, University of Malaya, Kuala Lumpur, 50603, Malaysia
[c] Department of Chemical Engineering, Faculty of Engineering, University of Malaya, Kuala Lumpur, 50603, Malaysia
[d] Department of Mechanical Engineering, King Fahd University of Petroleum and Minerals, Dhahran, 31261, Saudi Arabia
[e] Interdisciplinary Research Center for Intelligent Manufacturing & Robotics, King Fahd University of Petroleum and Minerals, Dhahran 31261, Saudi Arabia
[f] Department of Mechanical Engineering, Southern Taiwan University of Science and Technology, Tainan 701, Taiwan, R.O.C
[g] Sustainability Science and Engineering Program, Tunghai University, Taichung 407, Taiwan, R.O.C

ARTICLE INFO

Keywords:
Metallic glass
Biomaterials
Laser cladding
In-vitro bioactivity

ABSTRACT

The commonly used metallic biomaterials fail to prove durability for orthopedics due to their lack of biocompatibility and poor bioactivity which weakens the bonding to bones. Metallic glasses (MGs) have attracted attention as an alternative biomaterial for orthopedics owing to their superior mechanical properties and acceptable biocompatibility. Nevertheless, their uses are limited due to geometrical constraints and brittleness. In this research, the in-vitro bioactivity of laser cladded FeCrMoCB MG on nickel-free stainless-steel was investigated. The proposed MG coating exhibited a remarkable in-vitro bioactivity behavior without prior treatment after immersion in simulated body fluid which is a key factor for better osseointegration. The surface morphology showed that apatite nucleated from the first day and completely covered the surface after 21 days. The energy dispersive spectroscopy spectra showed an increase in the Ca/P ratio from 0.51 at 3 days to 1.61 at 21 days, thus approaching the stoichiometric ratio of bone apatite. The infra-red examination revealed the existence of Ca^{+2}, PO_4^{-2} and OH^{-} indicating the nucleation of brushite and B-type apatite. Additionally, the X-ray diffraction examination revealed the existence of amorphous and nanocrystalline calcium phosphates. These results show the potential of FeCrMoCB MGs as a promising bioactive coating for excellent osseointegration of metallic implants with bone tissue.

Abbreviations

MG	Metallic glass
SBF	Simulated body fluid
XRD	X-ray diffraction
SEM	Scanning electron microscope
EDS	Energy-dispersive spectroscopy
FTIR	Fourier-Transform infra-red
CL	Coating layer
DI	deionized

1. Introduction

Bioactivity describes the interaction of a biomaterial with bone-tissue upon exposure, i.e., the initiation and formation of apatite-like layer at the biomaterial-living tissue interface. It also describes the ability of the implant material to set up a chemical bonding with the host tissue. Thus, bioactivity can be a key property to promote the osseointegration which is vital for prolonging the durability of implanted device and reduce the possibility of implant separation [1–4].

Biomaterials can be metals, bioceramics, and biopolymers. Recently, metals and their alloys have been widely applied in biomedical implants

* Corresponding author.
** Corresponding author.
*** Corresponding author.
E-mail addresses: mahmoud.zakaria@eng.asu.edu.eg (M.Z. Ibrahim), ahsarhan@kfupm.edu.sa (A.A.D. Sarhan), hamdi@um.edu.my (M. Hamdi).

https://doi.org/10.1016/j.medengphy.2022.103782
Received 30 May 2021; Received in revised form 19 January 2022; Accepted 19 February 2022
Available online 21 February 2022

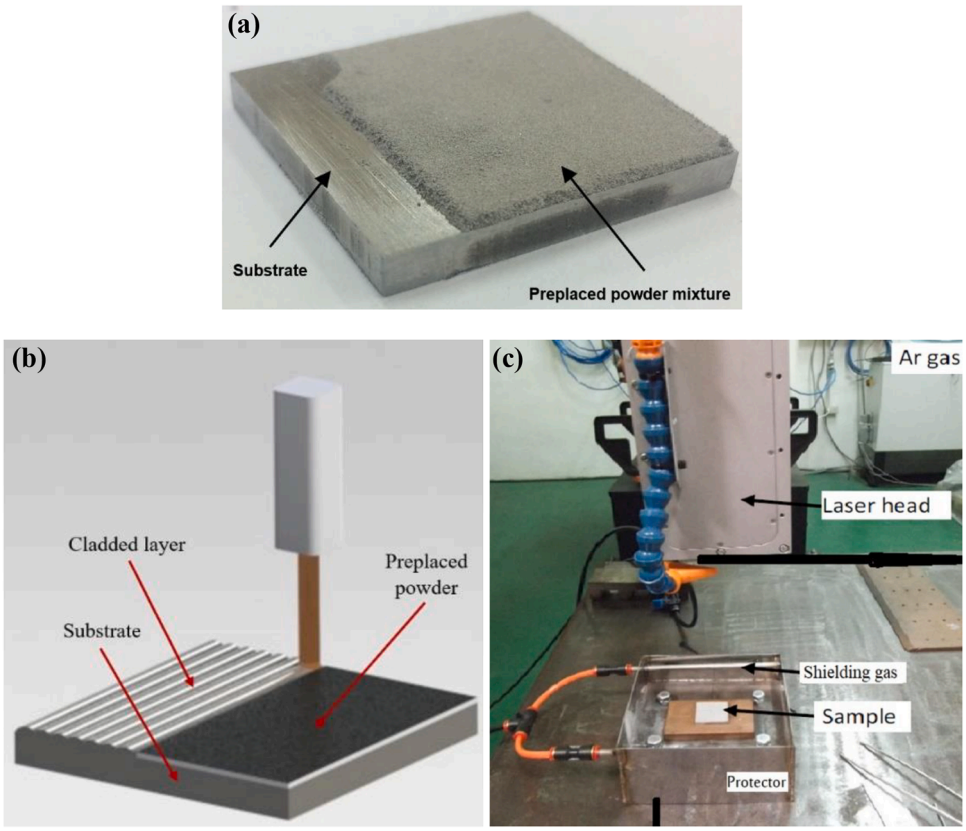

Fig. 1. (a) Preplaced powder on substrate, (b) Laser cladding process, (c) Laser cladding setup.

especially for load bearing implants and joint replacements [5,6]. Commonly used metallic biomaterials - 316 L stainless-steel, cobalt--chromium alloys and titanium-based alloys - demonstrate excellent fracture toughness and fatigue strength, improved corrosion resistance and acceptable cytocompatibility [7–9]. While there has been significant advancement in the properties of these alloys, metallic biomaterials have failed to provide good osseointegration with the bone which increases the possibility of implant loosening and separation [10,11].

Recently, researchers have focused on developing coating layers on metallic biomaterials to enhance their biocompatibility as well as bioactivity. Different coating materials and techniques have been introduced. Among these coating materials are hydroxyapatite and Bioglass which have been widely implemented for their excellent bioactivity and biocompatibility [12–14]. Nevertheless, the development of the coating layers is challenging. The difference in thermal expansion between the bioceramics and the metallic substrate causes cracking, problems in delamination and inadequate stability [15].

Metallic glasses (MGs) have recently gained more attention as coating layers on metallic substrates for biomedical applications because they show excellent wear and corrosion resistance, and acceptable biocompatibility [16,17]. Also, the similarity in elemental composition between the MGs and popular biomedical metallic alloys - Ti6V4Al, CoCrMo alloys and 316 L stainless-steel - leads to improved interfacial bonding and results in more stable coatings. Among the wide variety of researched MGs, Fe-based MG offer remarkable mechanical properties and excellent corrosion resistance – which are important properties for biomaterials – besides biocompatibility [18,19]. Moreover, based on our previous research, the Fe-based MG demonstrated excellent wear resistance in simulated body fluid better than Zr-based, Ti-based MGs and comparable to CoCr alloy which is known for excellent wear resistance [20]. In addition, Fe-based MG is inexpensive [21] making it a promising option as a coating layer for biomedical applications.

Various coating techniques were utilized to develop MG coatings using laser cladding and thermal spraying techniques [22–26]. Thermal spraying techniques induces problems in coating layer such as weak bonding and cracking [20]. While, laser cladding offered high adhesion bond but, on the other side, it induces crystalline phases within the amorphous structure [27–29].

In this research, the in-vitro bioactivity of laser cladded FeCrMoCB MG as a potentially superior wear-resistant coating for joint replacement implants [10, 30] was investigated. The proposed MG coating exhibited a remarkable in-vitro bioactivity behavior without prior treatment after immersion in simulated body fluid for 1, 3, 7, and 21 days. The apatite layer formed was confirmed via scanning electron microscopy, energy dispersive spectroscopy, Fourier-Transform infra-red spectroscopy and X-ray diffraction. The revealed behavior is expected to promote the osseointegration of the proposed biomaterial.

2. Materials and methods

2.1. Laser cladding of FeCrMoCB MG coating layer

Strips of nickel-free high nitrogen stainless-steel (3 mm thickness) - provided by Energietechnik GmbH, Germany - were cut into square coupons of 30×30 mm^2 using an abrasive cutting machine. The coupons were polished using SiC sandpaper 240-grit and washed with deionized water (DI) and ethanol in an ultrasonic bath, respectively. The cladding material is FeCrMoCB amorphous powder - produced by LiquidMetal® Coatings - with a nominal particle size distribution of 20–80 μm. The amorphous powder was preplaced evenly on the substrate, Fig. 1(a), to form a 400 μm thick layer for laser cladding as described in our previous work [30]. The laser cladding process was performed by scanning the whole surface, Fig. 1(b), with a high-power diode laser machine (LDF 4000–60, LaserLine, Germany, 4.4 kW rated power and 978–1025 ± 10 nm wavelength). The laser cladding parameters used in the current work are 2000 W laser power, 25 mm/s scanning speed, 4 × 6 mm laser spot,

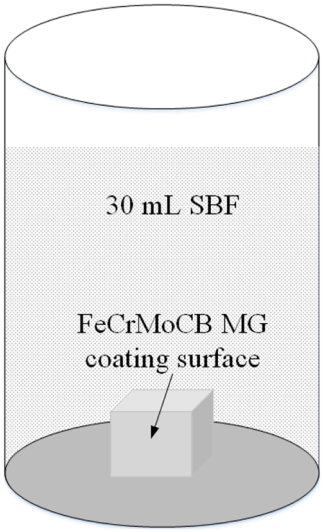

Fig. 2. In-vitro bioactivity setup showing the coating layer surface that is parallel to the direction of gravity.

and 25% overlap. These parameters have been selected based on our previous work [20,31,32] to ensure defect-free coating layer and best properties. A shielding Argon gas stream (10 L/min) was used to protect FeCrMoCB MG coating layer (CL) during the cladding process, Fig. 1(c).

2.2. Material characterization

The fabricated FeCrMoCB MG CL and the substrate (a 10×10 mm^2 coupons were cut, sanded by 240-gritt SiC sandpaper, then cleaned using DI water and ethanol in ultrasonic bath for 5 min., respectively) as well as the amorphous powder were examined using X-ray diffraction (XRD, Bruker D2 Phaser) – from 20° to 100° 2 θ at 3°/min scanning rate – and the obtained patterns were analyzed using X'Pert HighScore Plus suite (v3.0.3) [33]. To estimate the amorphous content and to quantify the phases, the constant background method – described in Eq. (1) [20] – and Rietveld's method [34] were used, respectively.

$$Amorphous\ content\% = \frac{integral\ area\ of\ the\ background}{integral\ area\ of\ original\ diffraction} \quad \text{(Eq. 1)}$$

2.2. Surface wettability test

The surface wettability can be evaluated through the measurement of the contact angle developed between the simulated body fluid (SBF) droplet and the tested surface. A sessile water-drop test was performed using a CAM-PlusR Contact angle goniometer. The test samples were polished to mirror-like finish using SiC sandpaper under stream of water, then polished using cloth disk and 40 nm alumina suspended in ethanol. Then, a 3 µl SBF droplet was put on the polished side of cladded samples and uncoated substrate. The contact angle was measured using imaging provided by attached camera. The recorded angle is the average value of three readings taken on each.

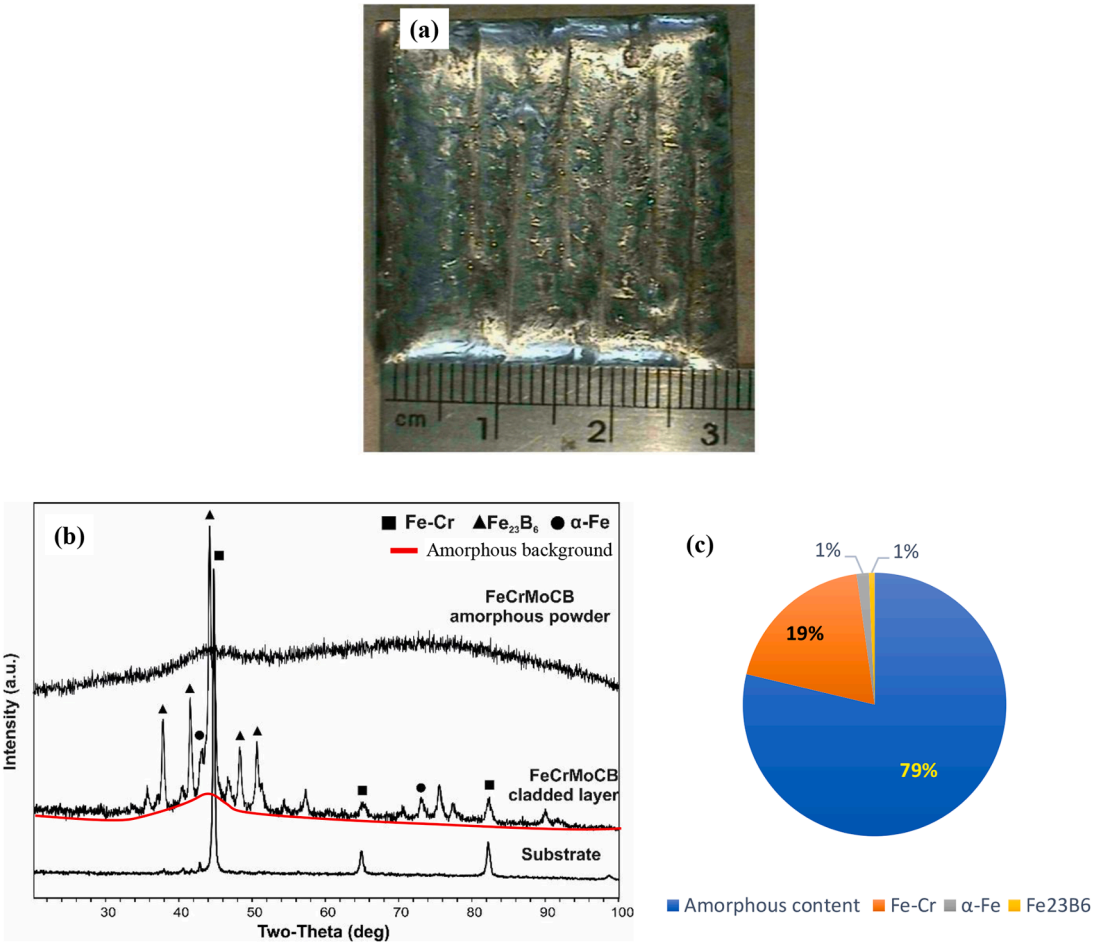

Fig. 3. (a) Sample after laser cladding, (b) XRD pattern of a FeCrMoCB CL, substrate and FeCrMoCB amorphous powder, and (c) Quantification of phase content of the laser cladded layer.

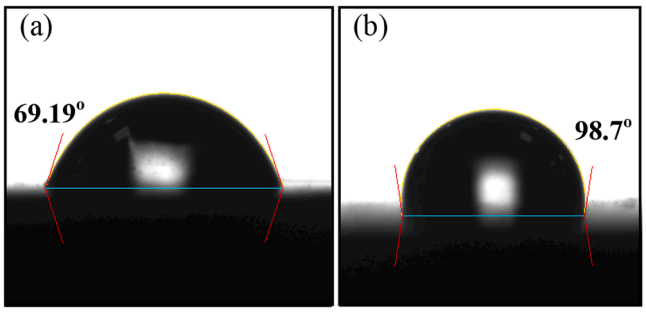

Fig. 4. Contact angle of 3 µl SBF drop on (a) FeCrMoCB MG CL and (b) nickel-free stainless-steel substrate.

2.3. The in-vitro bioactivity test of FeCrMoCB MG

The in-vitro bioactivity test was performed by immersion of samples in SBF. The SBF was prepared from lab-grade reagents according to a previous protocol proposed by Kokubo et al [3]. with pH of 7.4 and ion concentrations almost the same of the human blood plasma. Coupons of 9 × 9 mm^2 were cut from both the substrate and the laser cladded FeCrMoCB MG samples, and polished using sandpaper 240-gritt and then immersed in 30 ml SBF, Fig. 2, to ensure apatite formation on the surface rather than precipitation due to gravity. The samples were retained at 37±0.5 °C for 1 day, 3 days, 7 days, and 21 days. Kokubo et al. suggested 12, 24 and 120 hrs. for the in-vitro bioactivity test [3] while other researchers have used 14 [35,36] and 21 days [37].

Every two days, the test coupons were rinsed gently with deionized (DI) water and the SBF was replaced with a fresh one. After each designated period, the coupons were washed gently with DI water and dried in a desiccator.

2.4. The apatite layers characterization

To characterize the apatite layers, the coupons were initially coated with a conductive layer using ion sputter, then the morphology of the formed layer was examined by scanning electron microscopy (SEM, S-3000 N Hitachi, Japan). Then, elemental composition of the formed layer was checked using energy-dispersive spectroscopy (EDS, Falcon 60 EDS). Infrared light spectroscopy (FTIR-Spectrum 400, Perkin Elmer) was used to check the apatite layer formed on the samples. The IR spectra (4000–400 cm^{-1}) were recorded on a Fourier Transform spectrometer at a resolution of 2 cm^{-1}.

Furthermore, the apatite layer was gently scraped, put on a Si low background holder, and examined by XRD using 2° /min scanning rate in a range 0 to 50° of 2θ. Then, the obtained patterns were matched with the standard PDF2–2004 ICCD in X'Pert HighScore Plus Suite (v3.0.3) [33].

3. Results and discussion

3.1. Characterization of FeCrMoCB MG coating layer

Fig. 3(a) shows the sample after laser cladding. The sample presented successful cladding and the as cladded coating exhibited an almost homogeneous surface Fig. 3.(b) shows the XRD patterns of CL, substrate, and amorphous powder, while Fig. 3(c) shows the quantification of phase content of the laser cladded layer using the constant background method [38] and Rietveld's method [34]. As can be seen in Fig. 3(b), the XRD patterns showed a fully amorphous FeCrMoCB powder, while the substrate has typical crystalline structure. The laser cladded layer has a crystalline-amorphous composite structure with a high amorphous content (78.76%) as shown in Fig. 3(c). Fe-Cr and α-Fe (about 20%) were recognized as metallic crystalline phases and $Fe_{23}B_6$ as an intermetallic phase (less than 2%). Thus, the properties of the coating layer

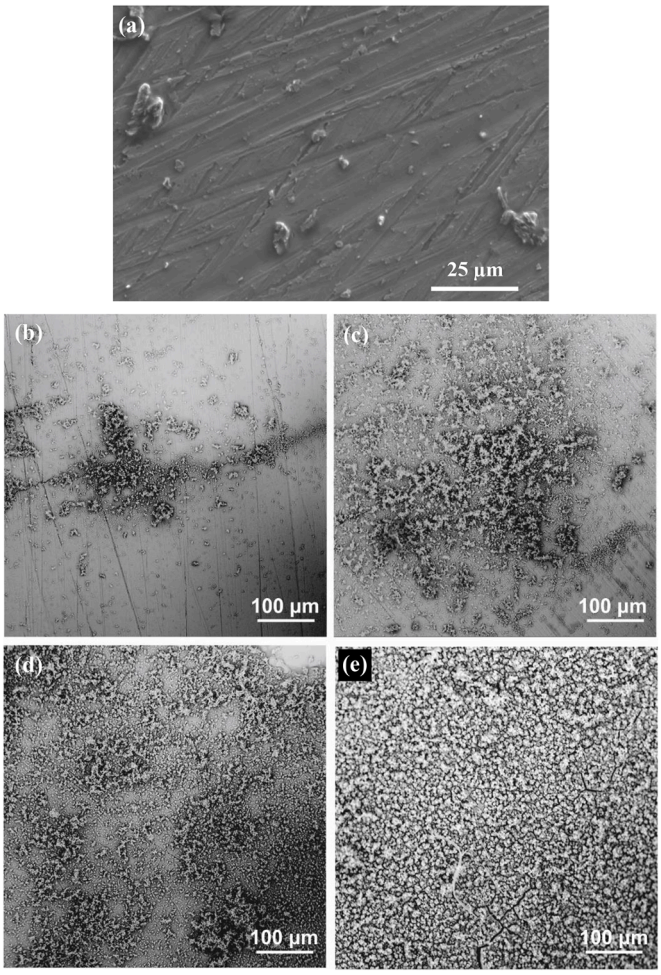

Fig. 5. SEM imaging of (a) Substrate (nickel-free stainless steel) morphology after 7 days of in-vitro bioactivity test and the apatite layer on the FeCrMoCB MG CL after (b) 1 day, (c) 3 days, (d) 7 days, and (e) 21 days.

are mostly affected by the amorphous structure and the metallic phases. The amorphous structure is recognized by the broad peak at 40–46°. Moreover, nanocrystalline phases were recognized in the coating layer which was demonstrated and discussed in our previous work [32].

3.2. The surface wettability test

Fig. 4 shows the contact angle of 3 µl SBF drop on (a) FeCrMoCB MG cladded layer and (b) nickel-free stainless-steel substrate. The wettability test showed that FeCrMoCB MG exhibited a contact angle of 69.19°±2.1° while the uncoated substrate recorded a contact angle of 98.7°±2.3°. This result confirms the higher hydrophilicity of FeCrMoCB MG surface as compared to the uncoated substrate, which in turn results in a higher surface energy [39] and consequently promotes the formation and growth of apatite on the coated surface [40–42]. Thus, FeCrMoCB MG shows better bioactivity behavior as compared to the uncoated substrate. Shen et al. also supported this finding and demonstrated that the crystallization of amorphous structure deteriorated the wettability which is regarded to higher surface energy of amorphous structure compared to crystalline one. If the surface has a high interfacial energy, roughness promotes wetting, and the liquid will spread within the corrugation (surface wicking). But for a low energy surface, roughness promotes repulsion; the liquid does not follow the surface corrugations but achieves its minimum at a position on top of the corrugation [43]. This explains the better wettability of FeCrMoCB MG CL compared to the substrate.

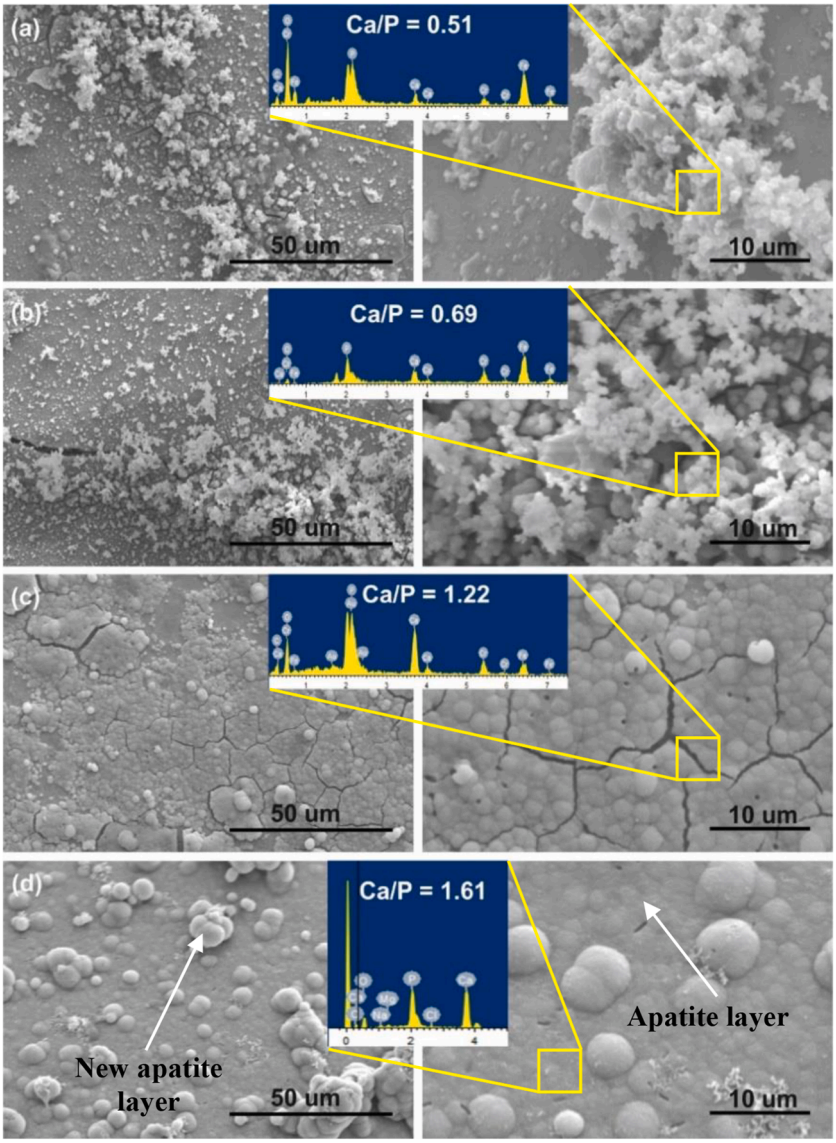

Fig. 6. Morphology and corresponding EDS spectra of apatite grown on FeCrMoCB MG CL after (a) 1 day, (b) 3 days, (c) 7 days, and (d) 21 days.

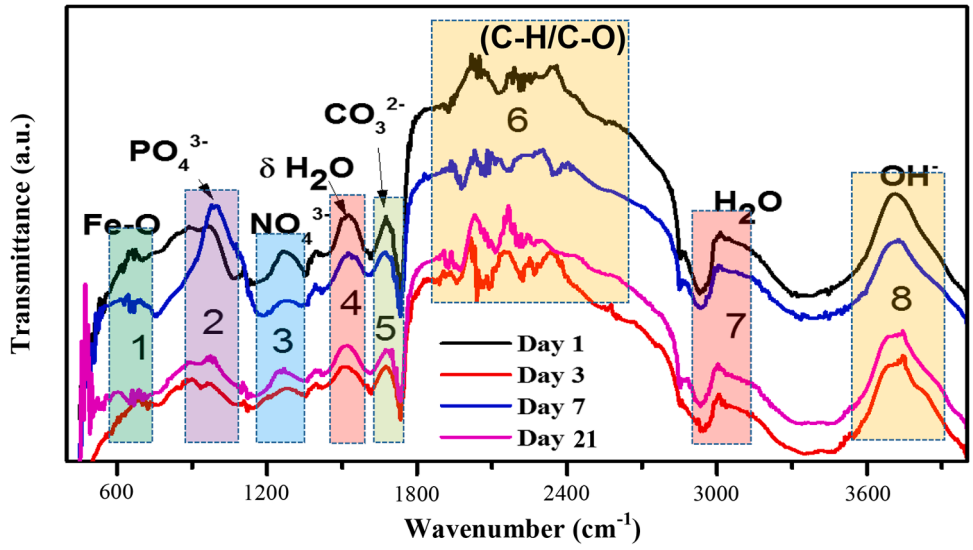

Fig. 7. FTIR spectra of apatite-like layer grown on the surface of FeCrMoCB amorphous MG samples monitored for 1-, 3-, 7- and 21-days period.

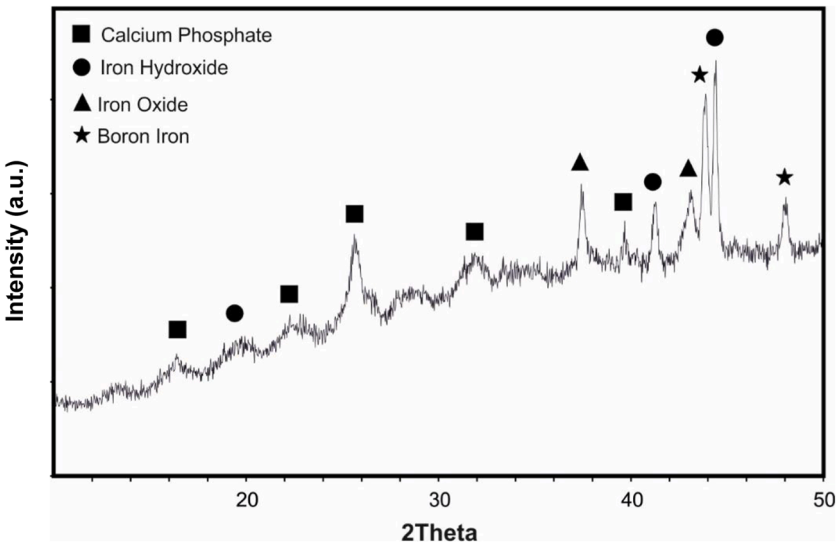

Fig. 8. XRD pattern of the apatite layer after 21 days of in-vitro bioactivity test.

3.3. The in-vitro bioactivity test

The SEM imaging of the surface morphology of the substrate and FeCrMoCB MG CL after the in-vitro bioactivity test is shown in Fig. 5. The substrate surface appeared to be clear with no evidence for apatite layer formation, Fig. 5(a). While the apatite layer nucleated from first day and grew rapidly to cover the whole surface of FeCrMoCB MG CL as appeared in Fig. 5 (b, c, d, and e) after in-vitro bioactivity test. The morphology and EDS spectra of apatite layer formed on FeCrMoCB MG CL after 1 day, 3 days, 7 days and 21 days is presented in Fig. 6. The EDS spectra showed that apatite-like layer is grown on the surface of the FeCrMoCB MG CL with existence of Ca and P, Fig. 6(a), (b), (c) and (d).

The EDS analysis showed that at 1 and 3 days of immersion, P and Ca are present, but the Ca/P ratio was below the stoichiometric ratio of bone apatite. However, after 7 days, Ca/P ratio increased to 1.25 and after 21 days became 1.61 approaching the stoichiometric ratio of bone apatite [39]. After 21 days, a new layer of apatite started to form on the top of the existed apatite layer. This could be described as a promising bioactive behavior. The FeCrMoCB MG exhibits bioactivity by forming Fe-OH groups which help the apatite formation and growth [44]. Moreover, boron enhances the bioactivity as it is known to be beneficial for healthy and growing bones [45,46].

3.4. Experimental FTIR apatite layer characterization

Fig. 7 shows the FTIR spectra of apatite-like layer grown on FeCrMoCB MG CL after 1, 3, 7 and 21 days of in-vitro bioactivity test. Generally, there are eight regions on the FTIR spectra that shows specific harmonics corresponding to Fe-O (region 1), PO_4^{3-}(region 2), NO_4^{3-}(region 3), δH_2O (region 4), CO_3^{2-}(region 5), C—H/C—O (region 6), H_2O (region 7), and OH^- (region 8) moieties detected on FeCrMoCB MG CL surface. These moieties have IR vibration centering at 660.4, 995.72, 1284.6, 1525.9, 1667.9, 1766.5–2796.6, 3037.1 and 3716.2 cm^{-1} respectively. The presence of PO_4^{3-}, NO_4^{3-}, and CO_3^{2-} moieties proves that apatite layer was grown on FeCrMoCB MG CL similar to hydroxyapatite according to previous report [47]. The *v*OH from iron species or adsorbed water showed a broad band at 3716.2 cm^{-1} [48]. The IR-absorption by PO_4^{3-} moiety after 7 days centered at 995.72 cm^{-1} with redshift of ~ 26.22 cm^{-1} from other days (1, 3 and 21) which occurred at 969.5 cm^{-1}. The IR-absorption by PO_4^{3-} indicates the stretching vibration of the P-O bond influenced by the carbonate (CO_3^{2-}) substitutions [49]. These carbonate substitutions (CO_3^{2-}) can replace phosphate ions to form B-type apatite – a carbonated apatite – which is the basic mineral found in the human bones [50]. The IR-absorption for H_2O which occurred at 3037.9 cm^{-1} indicates the formation of brushite ($CaHPO_4 \bullet 2H_2O$) [51]. This reveals a deficiency of calcium in the apatite layer and also shows non-stoichiometric apatite layer [52,53].

3.5. XRD of apatite layer formed on FeCrMoCB MG cladded layer

Fig. 8 shows the XRD pattern of the apatite particles - scraped from the FeCrMoCB MG CL - after 21 days of in-vitro bioactivity test. As can be seen in Fig. 8, the crystalline calcium phosphate is existed, besides iron hydroxide (Fe-OH) and iron oxide (Fe_2O_3). However, the recognized calcium phosphate peaks are referred to be nanocrystalline apatite [51]. From the EDS spectra (Fig. 6), it can be concluded that the amorphous component is amorphous calcium phosphate with Ca/P 1.61. The Fe-OH phase serves as nucleation site for growing appetite layer as illustrated by Qin et al [44]..

It can be postulated that the change in phase of Fe from crystalline to amorphous improved bioactivity. Therefore, the amorphous phase exhibited Fe at short range of atomic order hence providing better wettability. Consequently, the surface energy is higher and completely isotropic there by promoting the formation of Fe-OH phase. The Fe-OH phase was confirmed by the Fe-O vibration which is found at 660.4 cm^{-1}. Accordingly, Fe-OH serves as a nucleation sites for growth of Ca^{+2} and PO_4^{-2} into apatite. These results are significant in revealing the good bioactivity of the presented FeCrMoCB MG CL and also highlight its outstanding potential for bone-implant applications.

4. Conclusion

In this research work, the in-vitro bioactivity of laser cladded FeCrMoCB MG is investigated as potential material for excellent osseointegration in orthopedics. The laser cladded FeCrMoCB MG – having 78.76% amorphous phase – proved better wettability properties compared to uncoated nickel-free stainless-steel substrate. The cladded layer showed good in-vitro bioactivity in SBF and nucleation of apatite from first day without prior treatments. After 21 days, the apatite layer covered the whole surface with Ca/P 1.61 approaching the bone stoichiometric ratio of apatite. FTIR analysis showed existence of OH^-, PO_4^{-2} and Ca^{+2} on the surface confirming the existence of apatite layer. The analysis revealed formation of B-type apatite and brushite which have deficiency of calcium in the bone-like apatite. The XRD examination revealed the formation of nanocrystalline and amorphous calcium

phosphate, besides the existence of Fe-OH phase. These results are indicating that FeCrMoCB MG has promising bioactivity behavior and can be a promising implant material for better osseointegration in orthopedic implants.

Funding

This research work is funded by the King Fahd University of Petroleum & Minerals (KFUPM) under Funding Grant (DSR) Project Code: DF191046 and by University of Malaya under the RU Geran – Faculty program, project no. GPF062A-2020.

Declaration of Competing Interests

None declared

Ethical approval

Work on human beings that is submitted to *Medical Engineering & Physics* should comply with the principles laid down in the Declaration of Helsinki; Recommendations guiding physicians in biomedical research involving human subjects. Adopted by the 18th World Medical Assembly, Helsinki, Finland, June 1964, amended by the 29th World Medical Assembly, Tokyo, Japan, October 1975, the 35th World Medical Assembly, Venice, Italy, October 1983, and the 41st World Medical Assembly, Hong Kong, September 1989. You should include information as to whether the work has been approved by the appropriate ethical committees related to the institution(s) in which it was performed and that subjects gave informed consent to the work.

Acknowledgement

This research work is funded by the King Fahd University of Petroleum & Minerals (KFUPM) under Funding Grant (DSR) Project Code: DF191046 and by University of Malaya under the RU Geran – Faculty program, project no. GPF062A-2020. The authors would like to acknowledge LiquidMetal® Coatings for supplying FeCrMoCB powder and Energietechnik Essen GmbH for supplying nickel-free stainless steel as free-samples. Also, authors acknowledge Southern Taiwan University of science and technology and University of Malaya for providing technical support.

References

[1] Hench LL. Bioglass: 10 milestones from concept to commerce. J Non Cryst Solids 2016;432:2–8. https://doi.org/10.1016/j.jnoncrysol.2014.12.038.
[2] Chien CS, Liu CW, Kuo TY, Wu CC, Hong TF. Bioactivity of fluorapatite/alumina composite coatings deposited on Ti6Al4V substrates by laser cladding. Appl Phys A 2016;122:303. https://doi.org/10.1007/s00339-016-9788-1.
[3] Kokubo T, Takadama H. How useful is SBF in predicting in vivo bone bioactivity? Biomaterials 2006;27:2907–15. https://doi.org/10.1016/j.biomaterials.2006.01.017.
[4] Zafar MS, Farooq I, Awais M, Najeeb S, Khurshid Z, Zohaib S. Bioactive surface coatings for enhancing osseointegration of dental implants. Biomed Ther Clin Appl Bioact Glas 2019:313–29. https://doi.org/10.1016/B978-0-08-102196-5.00011-2.
[5] Pandey A, Awasthi A, Saxena KK. Metallic implants with properties and latest production techniques: a review. Adv Mater Process Technol 2020;6:167–202. https://doi.org/10.1080/2374068X.2020.1731236.
[6] Kocich R, Lowe TC, Kunc L. Advances in metals and alloys for joint replacement. Prog Mater Sci 2017;88:232–80. https://doi.org/10.1016/j.pmatsci.2017.04.002.
[7] Hanawa T. Evaluation techniques of metallic biomaterials in vitro evaluation techniques of metallic biomaterials in vitro. Sci Technol Adv Mater 2002:289–95.
[8] Prasad K, Bazaka O, Chua M, Rochford M, Fedrick L, Spoor J, Symes R, Tieppo M, Collins C, Cao A, Id DM, Ostrikov KK, Bazaka K. Metallic biomaterials : current challenges and opportunities. Materials (Basel) 2017;10:1–33. https://doi.org/10.3390/ma10080884.
[9] Tran PA, Sarker A, Tran N, Jeffery C, Rifai A, Fox K. Coatings on metallic implants for biomedical applications. Met Biomater Process Med Device Manuf. 2020:359–85. https://doi.org/10.1016/b978-0-08-102965-7.00011-4.
[10] Park J, Lakes RS. Biomaterials: an introduction, third edit. New York, NY: Springer New York; 2007. https://doi.org/10.1007/978-0-387-37880-0_5.
[11] Chen Q, Thouas GA. Metallic implant biomaterials. Mater Sci Eng R Reports 2015;87:1–57. https://doi.org/10.1016/j.mser.2014.10.001.
[12] Ibrahim MZ, Sarhan AAD, Yusuf F, Hamdi M. Biomedical materials and techniques to improve the tribological, mechanical and biomedical properties of orthopedic implants – A review article. J Alloys Compd 2017;714:636–67. https://doi.org/10.1016/j.jallcom.2017.04.231.
[13] Pourhashem S, Afshar A. Double layer bioglass-silica coatings on 316L stainless steel by sol-gel method. Ceram Int 2014;40:993–1000. https://doi.org/10.1016/j.ceramint.2013.06.096.
[14] Mohseni E, Zalnezhad E, Bushroa AR, Hamouda Abdel Magid, Goh BT, Yoon GH. Ti/TiN/HA coating on Ti–6Al–4V for biomedical applications. Ceram Int 2015;41:14447–57. https://doi.org/10.1016/j.ceramint.2015.07.081.
[15] Brunello G, Elsayed H, Biasetto L. Bioactive glass and silicate-based ceramic coatings on metallic implants: open challenge or outdated topic? Materials (Basel) 2019;12:2929. https://doi.org/10.3390/ma12182929.
[16] Horton JA, Parsell DE. Biomedical potential of a zirconium-based bulk metallic glass. MRS Proc 2002;754. https://doi.org/10.1557/PROC-754-CC1.5. CC1.5.
[17] Schroers J, Kumar G, Hodges TM, Chan S, Kyriakides TR. Bulk metallic glasses for biomedical applications. JOM 2009;61:21–9. https://doi.org/10.1007/s11837-009-0128-1.
[18] Li D, Chen X, Hui X, Wang J, Jin P, Li H. Effect of amorphicity of HVOF sprayed Fe-based coatings on their corrosion performances and contacting osteoblast behavior. Surf Coatings Technol 2017;310:207–13. https://doi.org/10.1016/J.SURFCOAT.2016.12.092.
[19] Wang YB, Li HF, Zheng YF, Li M. Corrosion performances in simulated body fluids and cytotoxicity evaluation of Fe-based bulk metallic glasses. Mater Sci Eng C 2012;32:599–606. https://doi.org/10.1016/j.msec.2011.12.018.
[20] Ibrahim MZ, Sarhan AAD, Kuo TY, Hamdi M, Yusof F, Chien CS, Chang CP, Lee TM. Advancement of the artificial amorphous-crystalline structure of laser cladded FeCrMoCB on nickel-free stainless-steel for bone-implants. Mater Chem Phys 2019;227:358–67. https://doi.org/10.1016/j.matchemphys.2018.12.104.
[21] Ibrahim MZ, Sarhan AAD, Kuo TY, Yusuf F, Hamdi M, Chien CS. Investigate the effects of the substrate surface roughness on the geometry, phase transformation, and hardness of laser-cladded Fe-based metallic glass coating. Int J Adv Manuf Technol 2018;98:1977–87. https://doi.org/10.1007/s00170-018-2354-6.
[22] Zhang H, Hu Y, Hou G, An Y, Liu G. The effect of high-velocity oxy-fuel spraying parameters on microstructure, corrosion and wear resistance of Fe-based metallic glass coatings. J Non Cryst Solids 2014;406:37–44. https://doi.org/10.1016/J.JNONCRYSOL.2014.09.041.
[23] Basu A, Samant AN, Harimkar SP, Majumdar JD, Manna I, Dahotre NB. Laser surface coating of Fe-Cr-Mo-Y-B-C bulk metallic glass composition on AISI 4140 steel. Surf Coatings Technol 2008;202:2623–31. https://doi.org/10.1016/j.surfcoat.2007.09.028.
[24] Ibrahim MZ, Sarhan AAD, Kuo TY, Yusof F, Hamdi M. Characterization and hardness enhancement of amorphous Fe-based metallic glass laser cladded on nickel-free stainless steel for biomedical implant application. Mater Chem Phys 2019;235:121745. https://doi.org/10.1016/j.matchemphys.2019.121745.
[25] Lee K, Nam D-H, Lee S, Kim NJ. Hardness and wear resistance of Zr-based bulk metallic glass/Ti surface composites fabricated by high-energy electron beam irradiation. Surf Coatings Technol 2006;201:1620–8. https://doi.org/10.1016/j.surfcoat.2006.02.032.
[26] Cheng J, Wang B, Liu Q, Liang X. In-situ synthesis of novel Al-Fe-Si metallic glass coating by arc spraying. J Alloys Compd 2017;716:88–95. https://doi.org/10.1016/j.jallcom.2017.05.032.
[27] Lan X, Wu H, Liu Y, Zhang W, Li R, Chen S, Zai X, Hu T. Microstructures and tribological properties of laser cladded Ti-based metallic glass composite coatings. Mater Charact 2016;120:82–9. https://doi.org/10.1016/j.matchar.2016.08.026.
[28] Fernandes M. Laser cladding of Fe-based bulk metallic glasses, in: 23rd ABCM Int. Congr Mech Eng 2015. https://doi.org/10.20906/CPS/COB-2015-1854.
[29] Lu Y, Huang G, Wang Y, Li H, Qin Z, Lu X. Crack-free Fe-based amorphous coating synthesized by laser cladding. Mater Lett 2018;210:46–50. https://doi.org/10.1016/J.MATLET.2017.08.125.
[30] Ibrahim MZ, Sarhan AAD, Kuo TY, Yusuf F, Hamdi M, Chien CS. Investigate the effects of the substrate surface roughness on the geometry, phase transformation, and hardness of laser-cladded Fe-based metallic glass coating. Int J Adv Manuf Technol 2018;98:1977–87. https://doi.org/10.1007/s00170-018-2354-6.
[31] Ibrahim MZ, Sarhan AD, Shaikh MO, Kuo TY, Yusuf F, Hamdi M. Investigate the effects of the laser cladding parameters on the microstructure, phases formation, mechanical and corrosion properties of metallic glasses coatings for biomedical implant application. Addit Manuf Emerg Mater 2019:299–323. https://doi.org/10.1007/978-3-319-91713-9.
[32] Ibrahim MZ, Sarhan AAD, Kuo TY, Yusof F, Hamdi M. Developing a new laser cladded FeCrMoCB metallic glass layer on nickel-free stainless-steel as a potential superior wear-resistant coating for joint replacement implants. Surf Coatings Technol 2020;392:125755. https://doi.org/10.1016/j.surfcoat.2020.125755.
[33] T. Degen, M. Sadki, E. Bron, U. König, G. Nénert, The HighScore suite, (2014) pp S13–S18.
[34] Kniess CT, Cardoso De Lima J, Prates PB. The quantification of crystalline phases in materials: applications of Rietveld method (editor). In: Shatokha V, editor. Sintering-Methods prod. InTech; 2012. p. 293–316.
[35] Kung K-C, Chen J-L, Liu Y-T, Lee T-M. Fabrication and characterization of CaP-coated nanotube arrays. Mater Chem Phys 2015;153:110–6. https://doi.org/10.1016/j.matchemphys.2014.12.042.
[36] Moritz N, Vedel E, Ylänen H, Jokinen M, Hupa M, Yli-Urpo A, Nen È, Jokinen M, Hupa M, Moritz N, Vedel E, Yla H, Group PC. Characterisation of bioactive glass

coatings on titanium substrates produced using a CO 2 laser. J Mater Sci Mater Med 2004;15:787–94. https://doi.org/10.1023/B:JMSM.0000032819.64994.42.
[37] Chien CS, Liao ZY, Hong TF, Kuo TY, Chang CH, Yeh ML, Lee TM. Surface microstructure and bioactivity of hydroxyapatite and fluorapatite coatings deposited on Ti-6Al-4V substrates using Nd-YAG laser. J Med Biol Eng 2014;34:109–15. https://doi.org/10.5405/jmbe.1379.
[38] Manne B, Bontha S, Ramesh MR, Krishna M, Balla VK. Solid state amorphization of Mg-Zn-Ca system via mechanical alloying and characterization. Adv Powder Technol 2017;28:223–9. https://doi.org/10.1016/J.APT.2016.09.032.
[39] Yang Y, Paital SR, Dahotre NB. Effects of SiO2 substitution on wettability of laser deposited Ca-P biocoating on Ti-6Al-4V. J Mater Sci Mater Med 2010;21:2511–21. https://doi.org/10.1007/s10856-010-4105-6.
[40] Miyazaki T, Kim H-M, Kokubo T, Ohtsuki C, Kato H, Nakamura T. Mechanism of bonelike apatite formation on bioactive tantalum metal in a simulated body fluid. Biomaterials 2002;23:827–32. https://doi.org/10.1016/S0142-9612(01)00188-0.
[41] Kokubo T, Miyaji F, Kim HM, Nakamura T. Spontaneous formation of bonelike apatite layer on chemically treated titanium metals. J Am Ceram Soc 1996;79:1127–9. https://doi.org/10.1111/j.1151-2916.1996.tb08561.x.
[42] Minamikawa H, Ikeda T, Att W, Hagiwara Y, Hirota M, Tabuchi M, Aita H, Park W, Ogawa T. Photofunctionalization increases the bioactivity and osteoconductivity of the titanium alloy Ti6Al4V. J Biomed Mater Res Part A 2014;102:3618–30. https://doi.org/10.1002/jbm.a.35030.
[43] Shen P, Sun J, Yang J, Qi Y, Jiang Q. Wettability of amorphous and nanocrystalline Fe78B13Si9 substrates by molten Sn and Bi. Nanoscale Res Lett 2011;6:318. https://doi.org/10.1186/1556-276X-6-318.
[44] Qin C, Hu Q, Li Y, Wang Z, Zhao W, Louzguine-Luzgin DV, Inoue A. Novel bioactive Fe-based metallic glasses with excellent apatite-forming ability. Mater Sci Eng C 2016;69:513–21. https://doi.org/10.1016/J.MSEC.2016.07.022.
[45] Balasubramanian P, Büttner T, Pacheco VM, Boccaccini AR, Miguez Pacheco V, Boccaccini AR. Boron-containing bioactive glasses in bone and soft tissue engineering. J Eur Ceram Soc 2018;38:855–69. https://doi.org/10.1016/J.JEURCERAMSOC.2017.11.001.
[46] Hakki SS, Dundar N, Ali S, Hakki EE, Hamurcu M, Kerimoglu U, Baspinar N, Basoglu A, Nielsen FH, Kayis SA, Hakki EE, Hamurcu M, Kerimoglu U, Baspinar N, Basoglu A, Nielsen FH. Boron enhances strength and alters mineral composition of bone in rabbits fed a high energy diet. J Trace Elem Med Biol 2013;27:148–53. https://doi.org/10.1016/J.JTEMB.2012.07.001.
[47] Meejoo S, Maneeprakorn W, Winotai P. Phase and thermal stability of nanocrystalline hydroxyapatite prepared via microwave heating. Thermochim Acta 2006;447:115–20. https://doi.org/10.1016/j.tca.2006.04.013.
[48] Ruan HD, Frost RL, Kloprogge JT. The behavior of hydroxyl units of synthetic goethite and its dehydroxylated product hematite. Spectrochim Acta - Part A Mol Biomol Spectrosc 2001;57:2575–86. https://doi.org/10.1016/S1386-1425(01)00445-0.
[49] Antonakos A, Liarokapis E, Leventouri T. Micro-Raman and FTIR studies of synthetic and natural apatites. Biomaterials 2007;28:3043–54. https://doi.org/10.1016/j.biomaterials.2007.02.028.
[50] Ren F, Leng Y, apatite Carbonated. Type-A or Type-B? Key Eng Mater 2012:293–7. https://doi.org/10.4028/www.scientific.net/KEM.493-494.293.
[51] Drouet C. Apatite formation: why it may not work as planned, and how to conclusively identify apatite compounds. Biomed Res Int 2013;2013:490946. https://doi.org/10.1155/2013/490946.
[52] Raynaud S, Champion E, Bernache-Assollant D, Thomas P. Calcium phosphate apatites with variable Ca/P atomic ratio I. Synthesis, characterisation and thermal stability of powders. Biomaterials 2002;23:1065–72. https://doi.org/10.1016/S0142-9612(01)00218-6.
[53] Kwon SH, Jun YK, Hong SH, Kim HE. Synthesis and dissolution behavior of β-TCP and HA/β-TCP composite powders. J Eur Ceram Soc 2003;23:1039–45. https://doi.org/10.1016/S0955-2219(02)00263-7.